AD-A164 652 A LOOP ANTENNA FOR A VLF (VERY LOW FREQUENCY) SATELLITE TRANSMITTER..(U) AEROSPACE CORP EL SEGUNDO CA SPACE SCIENCES LAB H C KOONS ET AL. 30 SEP 85 1/1

UNCLASSIFIED TR-0084A(5723-01)-1 SD-TR-85-49 F/G 17/2.1 NL

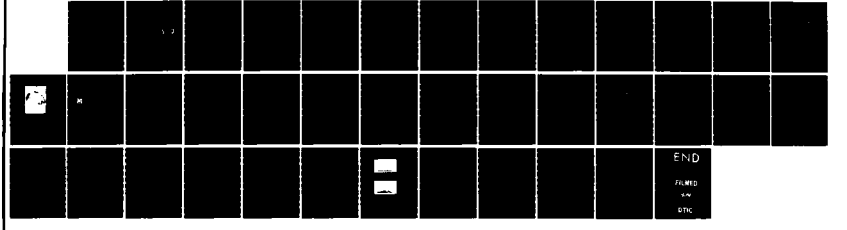

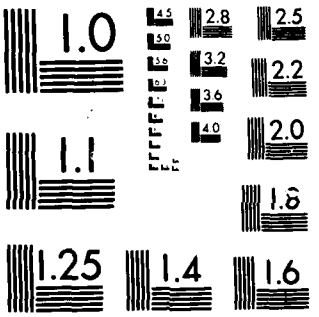

REPORT SD-TR-85-49

(12)

A Loop Antenna for a VLF Satellite Transmitter

Prepared by

H. C. KOONS, M. H. DAZEY, and D. C. PRIDMORE-BROWN
Space Sciences Laboratory
Laboratory Operations
The Aerospace Corporation
El Segundo, CA 90245

30 September 1985

Prepared for

NAVAL AIR SYSTEMS COMMAND
Philadelphia, PA 19111

SPACE DIVISION
AIR FORCE SYSTEMS COMMAND
Los Angeles Air Force Station
P.O. Box 92960, Worldway Postal Center
Los Angeles, CA 90009-2960

86 2 21 023

This report was submitted by The Aerospace Corporation, El Segundo, CA 90245, under Contract No. F04701-83-C-0084 with the Space Division, P.O. Box 92960, Worldway Postal Center, Los Angeles, CA 90009-2960. It was reviewed and approved for The Aerospace Corporation by H. R. Rugge, Director, Space Sciences Laboratory. Lieutenant Douglas R. Case, SD/YCM, was the project officer for the Mission- Oriented Investigation and Experimentation (MOIE) Program.

This report has been reviewed by the Public Affairs Office (PAS) and is releasable to the National Technical Information Service (NTIS). At NTIS, it will be available to the general public, including foreign nationals.

This technical report has been reviewed and is approved for publication. Publication of this report does not constitute Air Force approval of the report's findings or conclusions. It is published only for the exchange and stimulation of ideas.

Douglas R. Case

DOUGLAS R. CASE, Lt, USAF
MOIE Project Officer
SD/YCM

Joseph Hess

JOSEPH HESS, GM-15
Director, AFSTC West Coast Office
AFSTC/WCO OL-AB

UNCLASSIFIED

SECURITY CLASSIFICATION OF THIS PAGE (When Data Entered)

REPORT DOCUMENTATION PAGE	READ INSTRUCTIONS BEFORE COMPLETING FORM
1. REPORT NUMBER: SD-TR-85-49	2. GOVT ACCESSION NO.: AD A164 652
	3. RECIPIENT'S CATALOG NUMBER
4. TITLE (and Subtitle): A LOOP ANTENNA FOR A VLF SATELLITE TRANSMITTER	5. TYPE OF REPORT & PERIOD COVERED
	6. PERFORMING ORG. REPORT NUMBER: TR-0084A(5723-01)-1
7. AUTHOR(s): H. C. Koons, M. H. Dazey, D. C. Pridmore-Brown	8. CONTRACT OR GRANT NUMBER(s): F04701-83-C-0084
9. PERFORMING ORGANIZATION NAME AND ADDRESS: The Aerospace Corporation, El Segundo, Calif. 90245	10. PROGRAM ELEMENT, PROJECT, TASK AREA & WORK UNIT NUMBERS
11. CONTROLLING OFFICE NAME AND ADDRESS: Naval Air Systems Command, Philadelphia, PA 19111	12. REPORT DATE: 30 September 1985
	13. NUMBER OF PAGES: 32
14. MONITORING AGENCY NAME & ADDRESS (if different from Controlling Office): Space Division, Los Angeles Air Force Station, Los Angeles, Calif. 90009	15. SECURITY CLASS. (of this report): Unclassified
	15a. DECLASSIFICATION/DOWNGRADING SCHEDULE

16. DISTRIBUTION STATEMENT (of this Report)

Approved for public release; distribution unlimited.

17. DISTRIBUTION STATEMENT (of the abstract entered in Block 20, if different from Report)

18. SUPPLEMENTARY NOTES

19. KEY WORDS (Continue on reverse side if necessary and identify by block number)

Antenna impedance
Magnetic antenna
Plasma
Satellite VLF transmitter

20. ABSTRACT (Continue on reverse side if necessary and identify by block number)

The Space Sciences Laboratory of The Aerospace Corporation is currently defining an experiment to test a loop antenna configuration as a very low frequency (VLF) transmitter in the ionosphere. The experiment is sponsored by the Naval Air Systems Command. The primary objectives of the experiment are to validate existing models for radiation by a loop antenna and to study the performance of the antenna in the ionospheric plasma. The antenna will be carried into orbit in the payload bay of the Space Shuttle. During the radiation tests it will be deployed above the payload bay by the

DD FORM 1473 (FACSIMILE)

AIR FORCE, 86145/31-1-86 - 100

UNCLASSIFIED

SECURITY CLASSIFICATION OF THIS PAGE (When Data Entered)

19. KEY WORDS (Continued)

20. ABSTRACT (Continued)

remote manipulator system. A VLF receiver aboard a subsatellite will be used to map the radiation pattern of the antenna by measuring the field intensities at distances of 1 to 100 km from the transmitter. Calculations predict that the antenna impedance will only be slightly modified by the plasma and that the link to the receiver can be closed at distances well beyond 100 km. A one-third scale model of the antenna has been constructed. Impedance measurements have been made on the model in a 5-m diameter space plasma simulation chamber at NASA Lewis Research Center. The measurements confirm that the reactance of the antenna in an ionospheric plasma is essentially identical to its free space self-inductance. The effective series resistance of the circuit increases with frequency. The losses are attributed to power transferred to plasma turbulence.

PREFACE

The authors are indebted to Lou Corpas, Bob Vetrone, Norm Grier and the NASA Lewis Research Center personnel who lent their ready assistance to us for the tests performed at their facility.

We would like to thank Bobby Baldree from Aerospace for his help with the tests. We would also like to thank Bob Holzworth for his efforts in locating a suitable vacuum chamber for the tests.

CONTENTS

PREFACE..... 1

I. INTRODUCTION..... 7

II. BACKGROUND.. 9

III. ANTENNA CONFIGURATION..... 11

IV. RADIATION..... 15

V. PLASMA CHAMBER TESTS..... 27

VI. SUMMARY..... 37

REFERENCES..... 39

FIGURES

1. Concept of the NASC-201 Experiment..... 12

2. Photograph of the One-third Scale Model used in the Plasma Chamber Simulation Measurement..... 13

3. Electrical Block Diagram of the NASC-201 Experiment..... 14

4. Magnetic Field Intensity at a Distance of 100 km in the Ionosphere for a Transmitter Frequency of 100 Hz as a Junction of the Wave-normal Angle of the Whistler-mode Vector..... 16

5. Index of Refraction in the Plasma for a Frequency of 1000 Hz..... 18

6. Magnetic Field Intensity at a Distance of 100 km in the Ionosphere for a Transmitter Frequency of 1000 Hz..... 19

7. Magnetic Field Intensity at a Distance of 100 km in the Ionosphere for a Transmitter Frequency of 100 Hz plotted as a Function of the Electron Density at the Transmitter..... 20

8. Magnetic Field Intensity at a Distance of 100 km in the Ionosphere for a Transmitter Frequency of 1000 Hz plotted as a Function of the Geomagnetic Field Strength at the Transmitter..... 21

9. Concepts Involved in Transionospheric Propagation at VLF..... 23

10. The Magnetic Field Intensity at the Surface Directly Below the Exit Point from the Ionosphere..... 24

11. Antenna Current as a Function of Frequency at Two Voltage Levels..... 29

12. Resonant Frequency of the Antenna Circuit..... 31

FIGURES (Continued)

13. Histogram of the Antenna Circuit Series Resistance at Resonance for the Five Frequencies and Three Plasma Conditions Used in the Plasma Chamber Tests..... 33

14. Wave Spectrum in Plasma in the Frequency Range from 0 to 20 MHz..... 34

I. INTRODUCTION

Both the Navy and NASA have objectives that require the radiation of significant amounts of power at very low frequencies (VLF) in the ionosphere. Electric dipole and magnetic loop antennas have been proposed as transmitting antennas.

TRW is currently defining a VLF transmitter using an electric dipole for NASA's Waves In Space Plasmas (WISP) facility. WISP is to fly on the Space Plasma Lab 1 Mission tentatively scheduled for launch in 1988. At the Space Sciences Laboratory of The Aerospace Corporation we are defining a VLF transmitter using a multiturn loop antenna. The experiment is designated NASC-201. It is currently first on the U. S. Air Force Space Test Program experiment rankings list.

The loop antenna configuration and tests of a one-third scale model of the antenna in a space-plasma simulation chamber are described in this report.

II. BACKGROUND

The theory for the impedance, the radiation resistance, and the radiation pattern for both dipole and loop antennas at VLF in a plasma was formulated in the early 1970's [Wang and Bell, 1970, 1972; Bell and Wang, 1971].

Measurements of the impedance of electric dipole antennas in the low voltage linear regime have been performed using both rocket and satellite probes [Liephart et al., 1962; Shawhan and Gurnett, 1968; Grard and Tunaley, 1968; Gurnett et al., 1969; Koons et al., 1970]. These measurements showed that the impedance of the plasma sheath surrounding the antenna elements dominated the impedance at the antenna terminals. Shkarofsky [1972] developed a quasistatic nonlinear sheath model which he used to compute the impedance of an electric-dipole antenna driven at voltages much larger than plasma potential.

Measurements of the nonlinear impedance were made on a 32-m dipole at voltages up to 100 V peak-to-peak at seven frequencies from 400 Hz to 14 kHz on the OV1-21 satellite by Koons and McPherson [1974]. The magnitude of the impedance was in excellent agreement with Shkarofsky's model. However, the phase was found to advance with increasing voltage drive and increasing frequency. This phase advance implied an inductive reactance in the circuit. This result was contrary to existing nonlinear sheath models which predicted an increasing capacitive reactance as frequency and voltage increase [Shkarofsky, 1972; Baker et al., 1973].

The conclusion from the OV1-21 impedance measurements was that an electric-dipole antenna could not be resonated using a fixed reactance because nonlinear plasma effects caused significant changes in the impedance of the antenna circuit on a time scale that is shorter than the period of the applied signal. The theory for a loop antenna in an ionospheric plasma predicts that the resonant frequency will only shift about 1 part in 10^4 [Wang and Bell, 1972].

III. ANTENNA CONFIGURATION

The concept of the NASC-201 experiment is shown in Fig. 1. The experiment will fly on the Space Shuttle. The antenna will be deployed by the Remote Manipulator System (RMS) so that the antenna is held in the plasma above the payload bay. The radiation pattern shown in the figure represents a typical pattern in the ionosphere. The pattern is azimuthally symmetric about the magnetic field line. A subsatellite containing a VLF receiver and plasma diagnostics will measure the radiation intensity and radiation pattern to distances of 100 km from the transmitting antenna.

The antenna consists of about 100 turns of 3/8-in copper tubing. It is 3.3 m in diameter and 2.5 m long. A one-third scale model of the antenna is shown in Fig. 2.

An electrical block diagram of the transmitter system is shown in Fig. 3. It is currently planned to have the power amplifier and tuning network with the antenna on the RMS. This simplifies the electrical accommodation by passing direct-current primary power up the RMS rather than alternating-current, secondary power at much higher voltage. Four or five frequencies approximately an octave apart will be used. This simplifies the tuning circuit which will be a switchable capacitor bank.

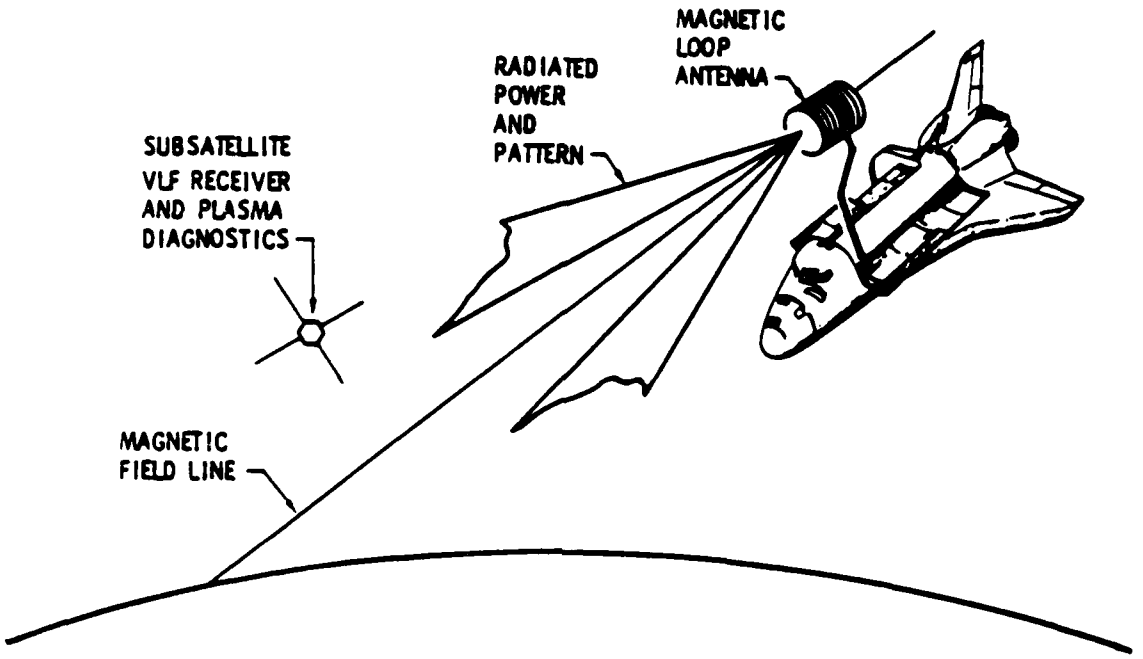

Fig. 1. Concept of the NASC-201 experiment. A subsatellite will be used to measure the signal strength and radiation pattern from a VLF antenna on the Space Shuttle.

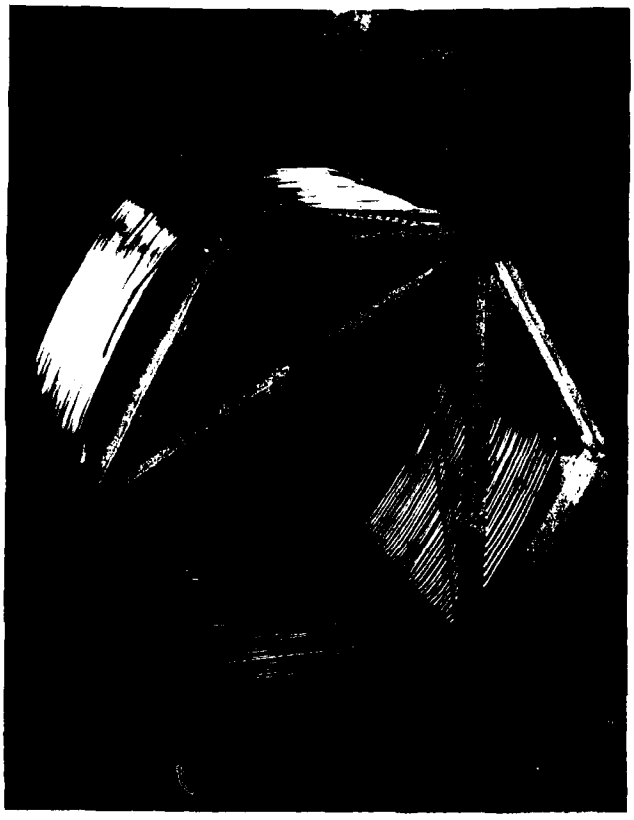

Fig. 2. Photograph of the one-third scale model used in the plasma chamber simulation measurements.

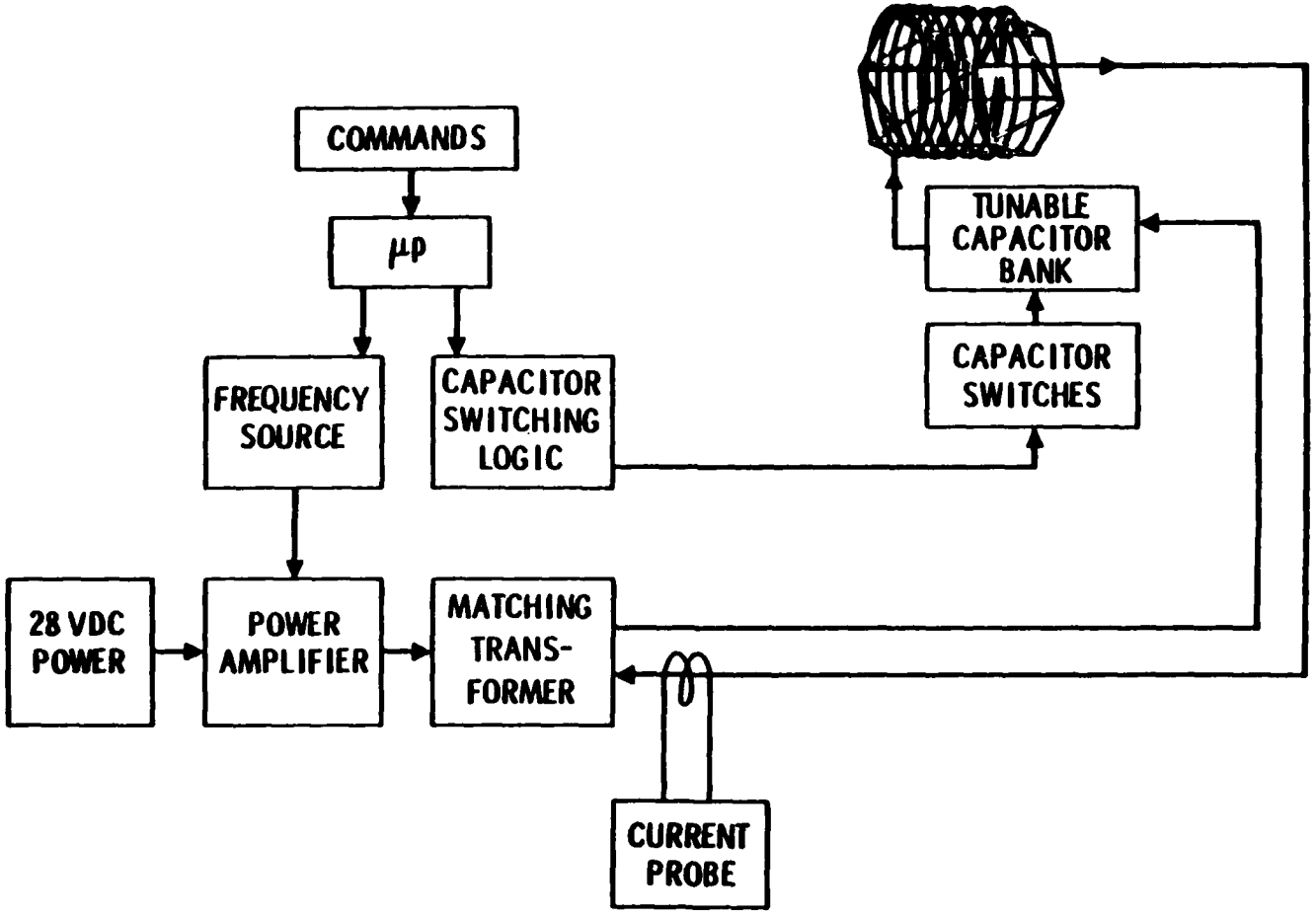

Fig. 3. Electrical block diagram of the NASC-201 experiment.

IV. RADIATION

Calculations of the radiation pattern and field intensity have been performed for several typical sets of ionospheric parameters. Fig. 4 shows the field intensity at 1 kHz at a distance of 100 km from the antenna as a function of the wave-normal angle of the radiated whistler-mode wave for the parameters listed in Table 1. The index of refraction of the medium for this case is shown in Fig. 5. The maximum signal intensity occurs at the inflection point in the index of refraction surface near a wave-normal angle of 60 deg where the wave normals are essentially parallel over a small angular range. In real space the energy propagates within a cone whose half-angle is approximately 20 deg. The data in Fig. 4 are replotted in Fig. 6 as a function of the polar angle in real space. The peak near 20 deg corresponds with the maximum at a wave-normal angle of 60 deg. The higher branch of the curve in Fig. 6 corresponds to wave-normal angles greater than 60 deg. The curve rises to a somewhat larger value then goes to zero at a polar angle of zero deg. The index of refraction of this upper branch is significantly larger than the index of refraction of the lower branch.

The magnetic field strength at a distance of 100 km in the ionosphere is plotted in Fig. 7 as a function of the electron density at the transmitter and in Fig. 8 as a function of the geomagnetic field strength at the transmitter. The received field is directly proportional to the electron density and inversely proportional to the geomagnetic field strength.

These results have important implications for the conduct of the flight experiment. First, within the ionosphere the signal is only expected to be detected within an angle of about 20 deg with respect to the local magnetic field direction. There is adequate link margin to measure the field intensity to 100 km in the ionosphere. Second, the received wave field will consist of two components - one with a wave-normal angle below about 60 deg and one with a wave-normal angle above 60 deg. The one with the wave-normal angle above 60 deg will be an order of magnitude stronger than the one below 60 deg and thus

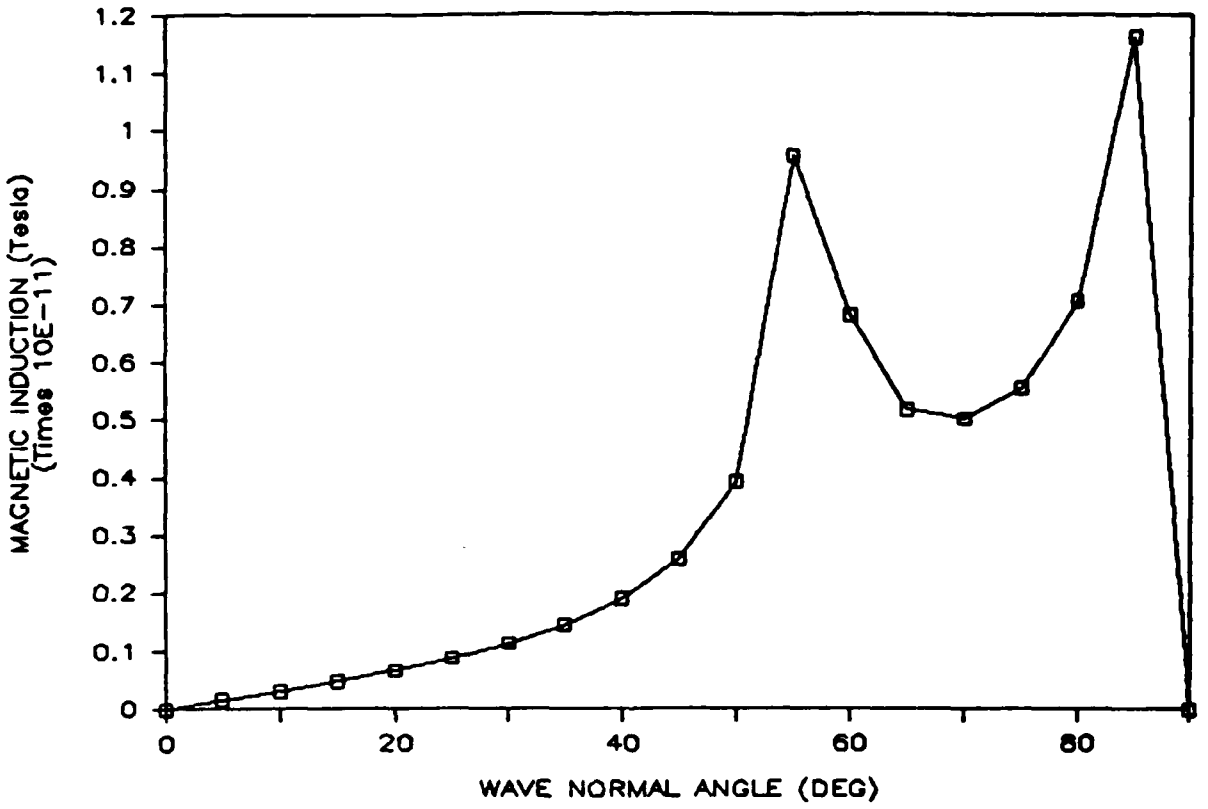

Fig. 4. Magnetic field intensity at a distance of 100 km in the ionosphere for a transmitter frequency of 1000 Hz as a function of the wave-normal angle of the whistler-mode vector.

Table 1. Ionospheric and Antenna Parameters Used for the Radiation Calculations

IONOSPHERE	
Electron Density	2.4×10^6 cm^{-3}
Magnetic Field	0.428 Gauss
Ion Charge	1
Mass Ratio	16
Height of Ionosphere	90,000 m
ANTENNA	
Antenna Current	30 amps
Azimuthal Angle	0 deg
Antenna Radius	1.65 m
Turns	100
Distance	100,000 m
Magnetic Moment	25,659 amp-m^2

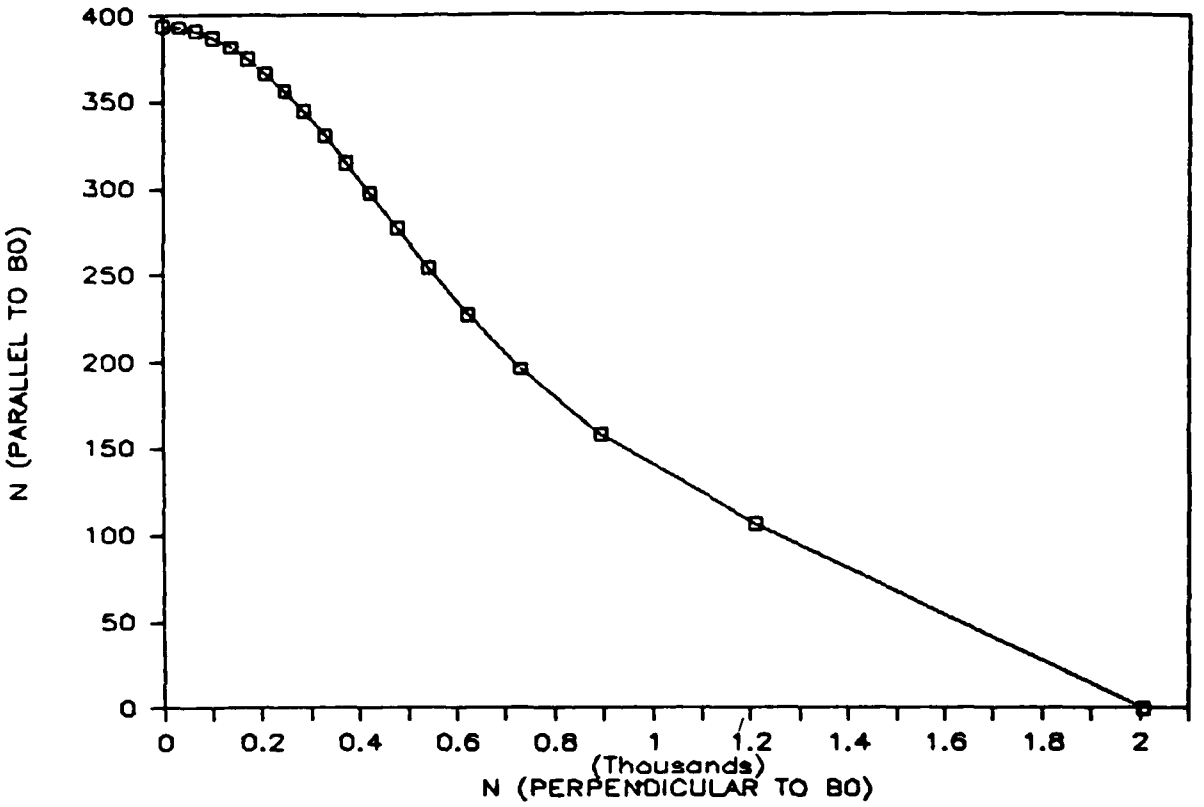

Fig. 5. Index of refraction in the plasma for a frequency of 1000 Hz.

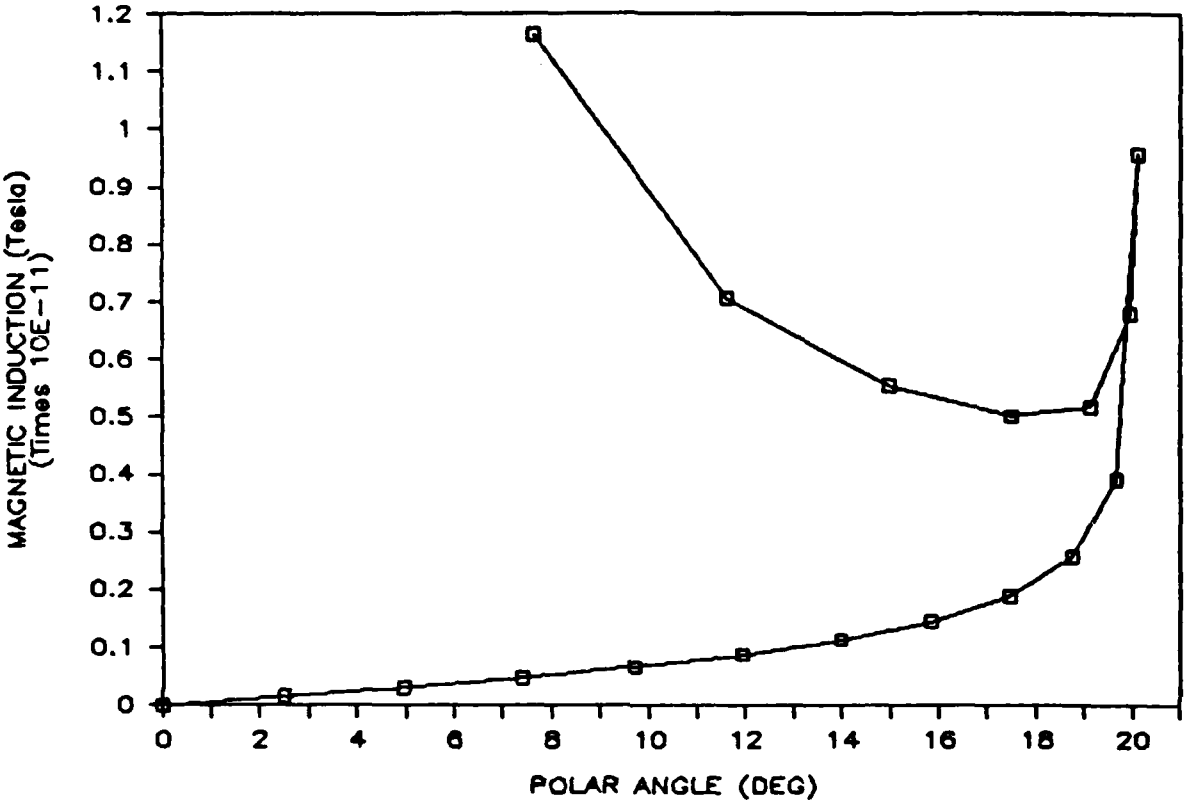

Fig. 6. Magnetic field intensity at a distance of 100 km in the ionosphere for a transmitter frequency of 1000 Hz. The field strength is plotted as a function of the angle between the geomagnetic field direction and the line-of-sight vector to the subsatellite.

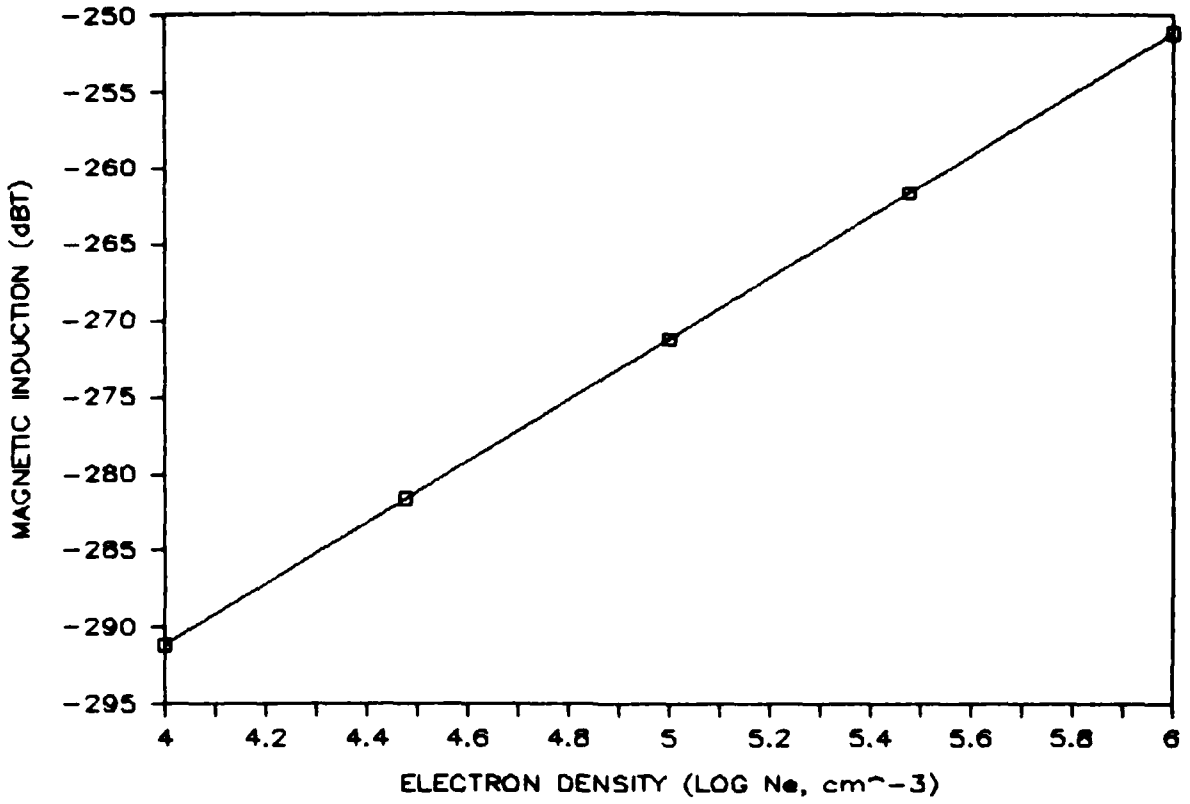

Fig. 7. Magnetic field intensity at a distance of 100 km in the ionosphere for a transmitter frequency of 1000 Hz plotted as a function of the electron density at the transmitter.

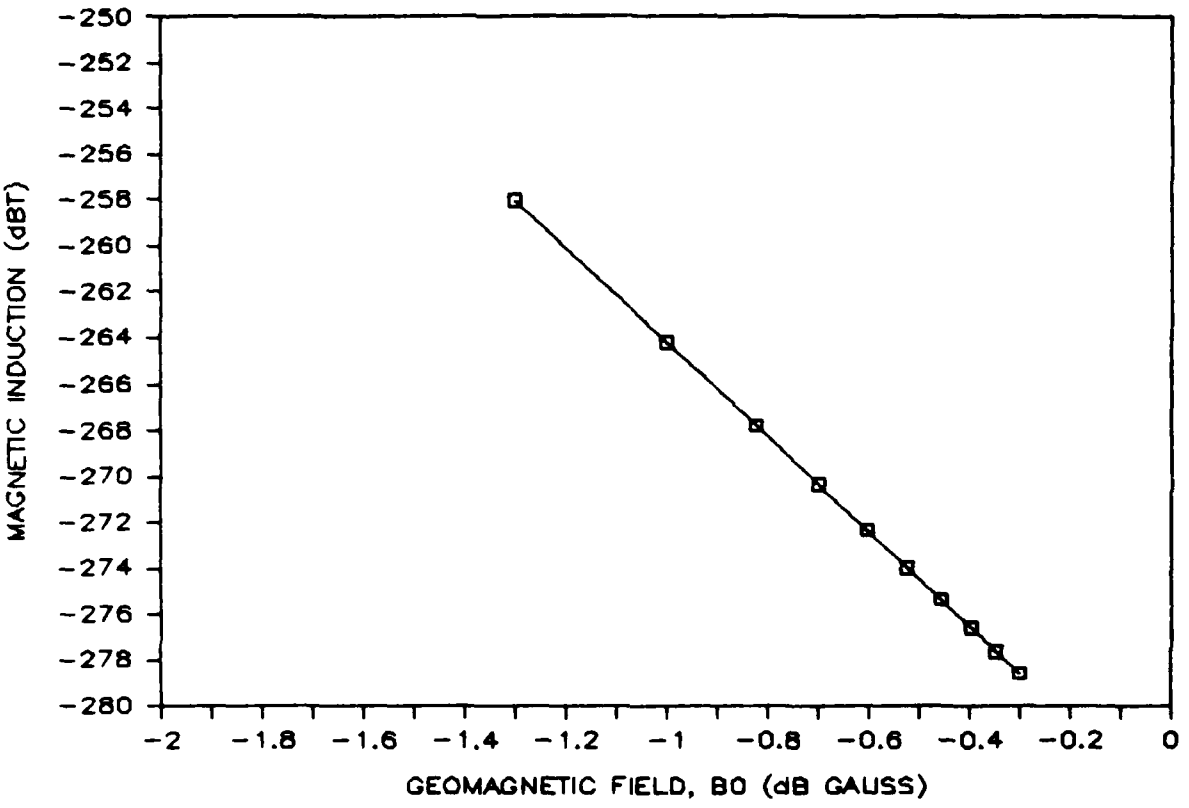

Fig. 8. Magnetic field intensity at a distance of 100 km in the ionosphere for a transmitter frequency of 1000 Hz plotted as a function of the geomagnetic field strength at the transmitter.

will dominate the signal at the subsatellite VLF receiver. For trans-ionospheric propagation the wave-normal angles near 60 deg are the most important because they will produce the largest signal in the earth-ionosphere waveguide. An important objective of the flight experiment then is to measure the amplitude of this maximum which occurs near a wave-normal angle of 60 deg. In physical space this is at the edge of the group-velocity cone at an angle of about 20 deg with respect to the local magnetic field.

Although the primary objective of the experiment is to measure the radiation pattern and field strengths in the ionosphere, a secondary objective is to attempt to detect the signal on the ground. Figure 9 shows the basic concepts involved. The most important consideration is the small size of the transmission cone between the ionosphere and the waveguide. Only a small fraction of the radiation emitted in the high refractive index medium can be transmitted across the boundary into the neutral atmosphere. Although a full wave treatment is required to obtain accurate numerical results, the basic concepts can be followed using a simple slab model in which the antenna is imbedded in a semi-infinite uniform medium representing the ionosphere and magnetosphere. The lower edge of the ionosphere is terminated at 90 km. The receiver is assumed to be at the surface directly below the exit cone. Note that this is not necessarily directly below the transmitter because the energy is propagating at an angle of 20 deg with respect to the local magnetic field until the radiation encounters the lower boundary of the ionosphere. If n_1 is the index of refraction in the ionosphere and n_2 in air, then $n_1 \gg n_2$ and propagating waves in the air can only result from waves in the ionosphere which have wave normals with angles within the transmission cone whose half-angle is:

$$\theta_t = \sin^{-1} (n_2/n_1)$$

In the slab model we assume that the signal spreads to a solid angle of 2π in the waveguide. Using this simple model we have computed the magnetic field strength at the surface for a variety of wave-normal angles and antenna pointing directions. Figure 10 shows the results for a signal frequency of

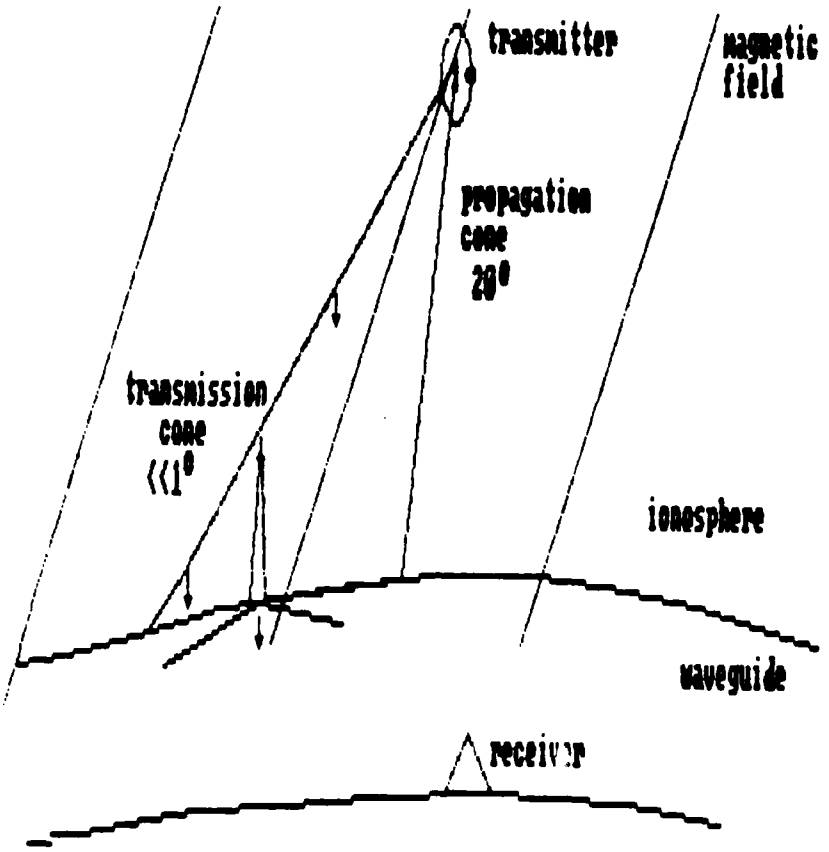

Fig. 9. Concepts involved in transionospheric propagation at VLF. Waves propagate from the ionosphere to the earth-ionosphere waveguide only within a small transmission cone whose size is determined from the index of refraction of the plasma at the transmitter.

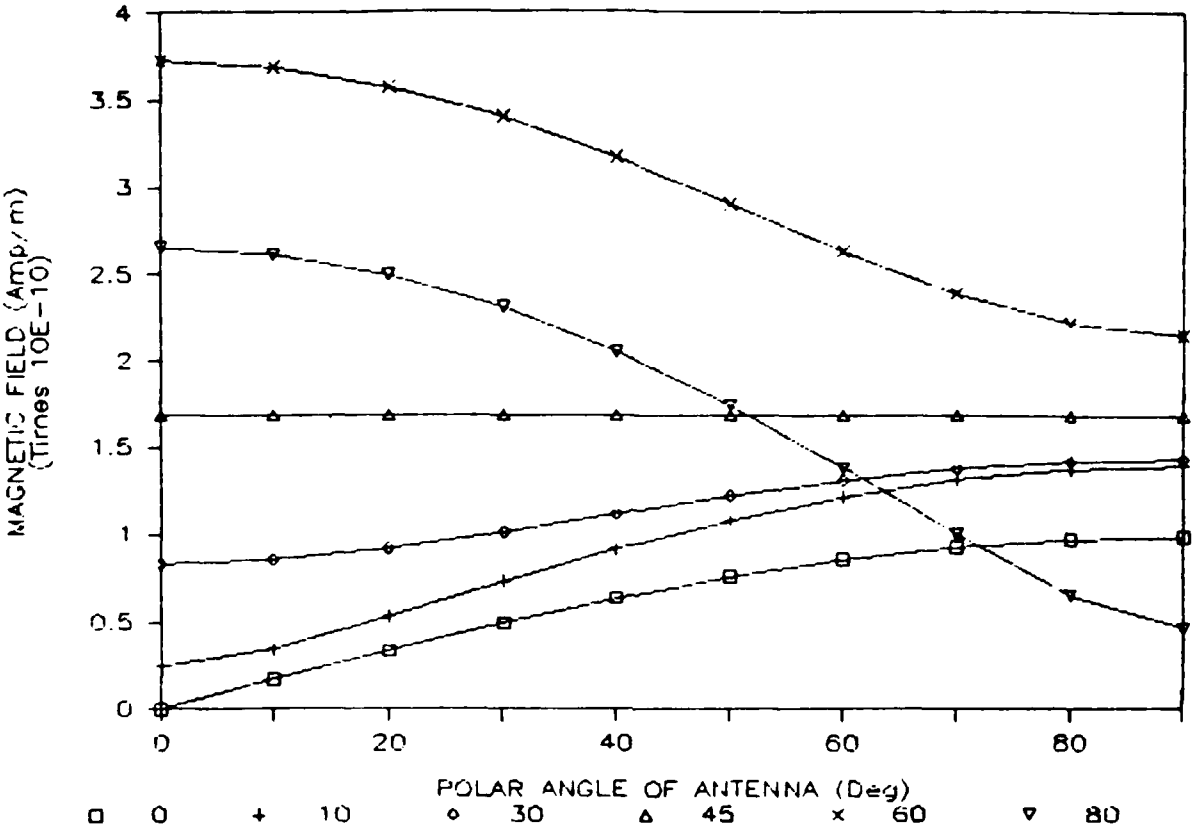

Fig. 10. The magnetic field intensity at the surface directly below the exit point from the ionosphere.

1 kHz. The abscissa is the polar angle of the antenna axis with respect to the local magnetic field direction. The largest signal over the entire range of polar angles occurs at the maximum in the radiation pattern near 60 deg wave-normal angle. Since the wave normal must be essentially vertical to be in the transmission cone, the maximum signal occurs geographically where the magnetic dip angle is the complement of the wave-normal angle. In this case that corresponds to a magnetic dip angle near 40 deg.

The signal strength at 500, 1000, and 2000 Hz is below the ambient noise at those frequencies. However the signal strength at 4000 Hz is computed to be above the ambient noise near the exit cone.

V. PLASMA CHAMBER TESTS

In order to test this concept for an antenna in a plasma, a scale-model loop antenna was operated in a 5-m diameter space plasma simulation chamber at the NASA Lewis Research Center. The antenna parameters are listed in Table 2. The objectives of the test were to measure the absolute value of the complex impedance, the resonant frequencies, and the near fields of the antenna. The thermal properties of the structure and plasma instabilities generated by the VLF fields were also measured.

The measurements were made in an argon ion plasma under two conditions. A relatively uniform density of 8×10^4 elec/cm^3 was produced using four plasma guns. A higher density of 1.2×10^6 elec/cm^3 was produced at the antenna by augmenting the plasma guns with a plasma thruster at one end of the chamber. The thruster produced a directed flow along the axis of the chamber with a density gradient of 10^6 elec/cm^3/m. The electron density and temperature were measured by four Langmuir probes placed about the antenna. In the low density plasma the electron temperature was 1.1 eV. In the high density plasma the temperature was 0.6 eV. Helmholtz coils provided a 0.4 G field parallel to the axis of the cylindrical vacuum chamber.

One of the major results of the measurements was the confirmation that the resonant frequency of the tuned antenna circuit is insensitive to the plasma density. Fig. 10 shows typical resonances in the antenna current for the antenna in the plasma. These measurements were made by sweeping the frequency at a constant amplifier voltage. Below a plasma wave instability threshold a smooth curve is obtained. Above that threshold, which occurs at an antenna current of 8.6 A r.m.s. in Fig. 10, the circuit resistance abruptly increases. There is only a slight shift in the resonant frequency. The resonant frequency for three different values of the tuning capacitance is shown in Fig. 11. Even in the absence of the plasma the resonant frequency depends upon the orientation of the antenna in the tank. The resonant frequency is slightly lower when the axis of the antenna is perpendicular to the axis of the tank. At 500 Hz the shift in the resonant frequency is smaller

Table 2. Scale-Model Antenna Parameters

Diameter	110 cm
Height	66 cm
Weight	60.5 kg
Copper Tubing	3/8 in O.D.
Turns	37
Structural Material	Lexan

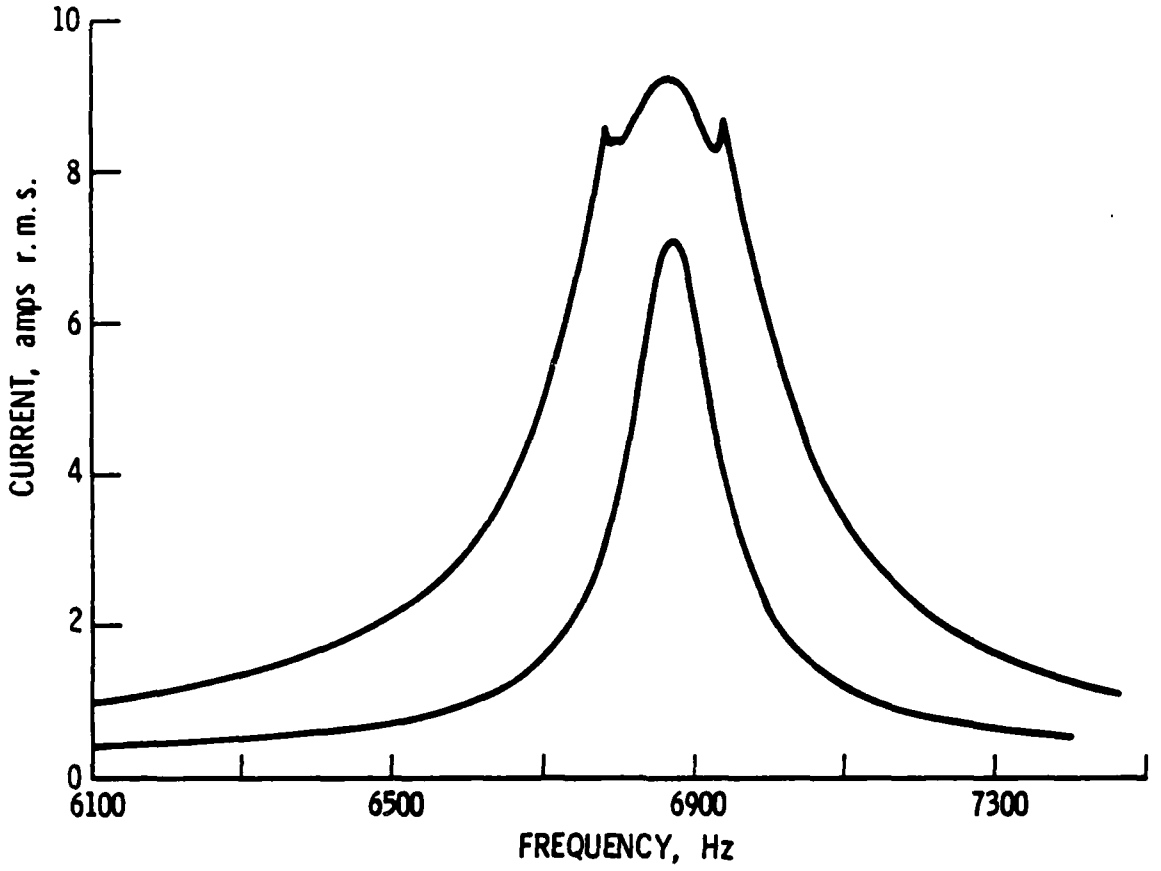

Fig. 11. Antenna current as a function of frequency at two voltage levels. The higher current curve shows the result of a sudden change of the Q of the resonance circuit at about 8.5 A.

than the resolution (~ 5 Hz) of the measuring instruments over the entire range of plasma densities and antenna orientations. At 7000 Hz there is a shift of about 20 Hz or 3 parts in 10^3 at the highest density.

The series resistance of the circuit at resonance is the r.m.s. voltage divided by the r.m.s. current. The histogram in Fig. 12 shows this series circuit resistance as a function of frequency for the antenna in vacuum and for the two plasma densities. Table 3 shows the drive current for each condition. At the lower frequencies the resistance is almost unaffected by the plasma. At the higher frequencies the resistance increases as the density increases.

Using available tuning capacitors, the resonant frequency of the circuit could only be changed in discrete steps that were approximately an octave apart. For this reason it was not possible to sweep in frequency to look for impedance effects near the lower-hybrid-resonance frequency (LHR). The LHR was 3.7 kHz at the lower density and 4.1 kHz at the higher density. The data in Fig. 12 suggest that the increase in series resistance may in part be related to the LHR. Well below the LHR the resistance was insensitive to density, while above the LHR, in the frequency range where the index of refraction has a resonance cone, the resistance increased with density. This large increase in series resistance is not predicted by existing theory [Wang and Bell, 1972].

The increase in circuit resistance was accompanied by an increase in plasma turbulence. Fig. 13 shows the plasma wave spectrum from 0 to 20 MHz on a small electric field probe in the plasma. The data were taken at a nominal electron density of 1.2×10^6 elec/cm^3. Fig. 14a shows the background spectrum in the plasma in the absence of antenna current.

The line near 9 MHz in Fig. 14a and 12 MHz in Fig. 14b is an EMI line that is not related to the antenna measurements. The feature from 14 to 16 MHz appears when the plasma thruster is turned on. It is most likely related to the plasma frequency in the higher density region near the aperture of the thruster.

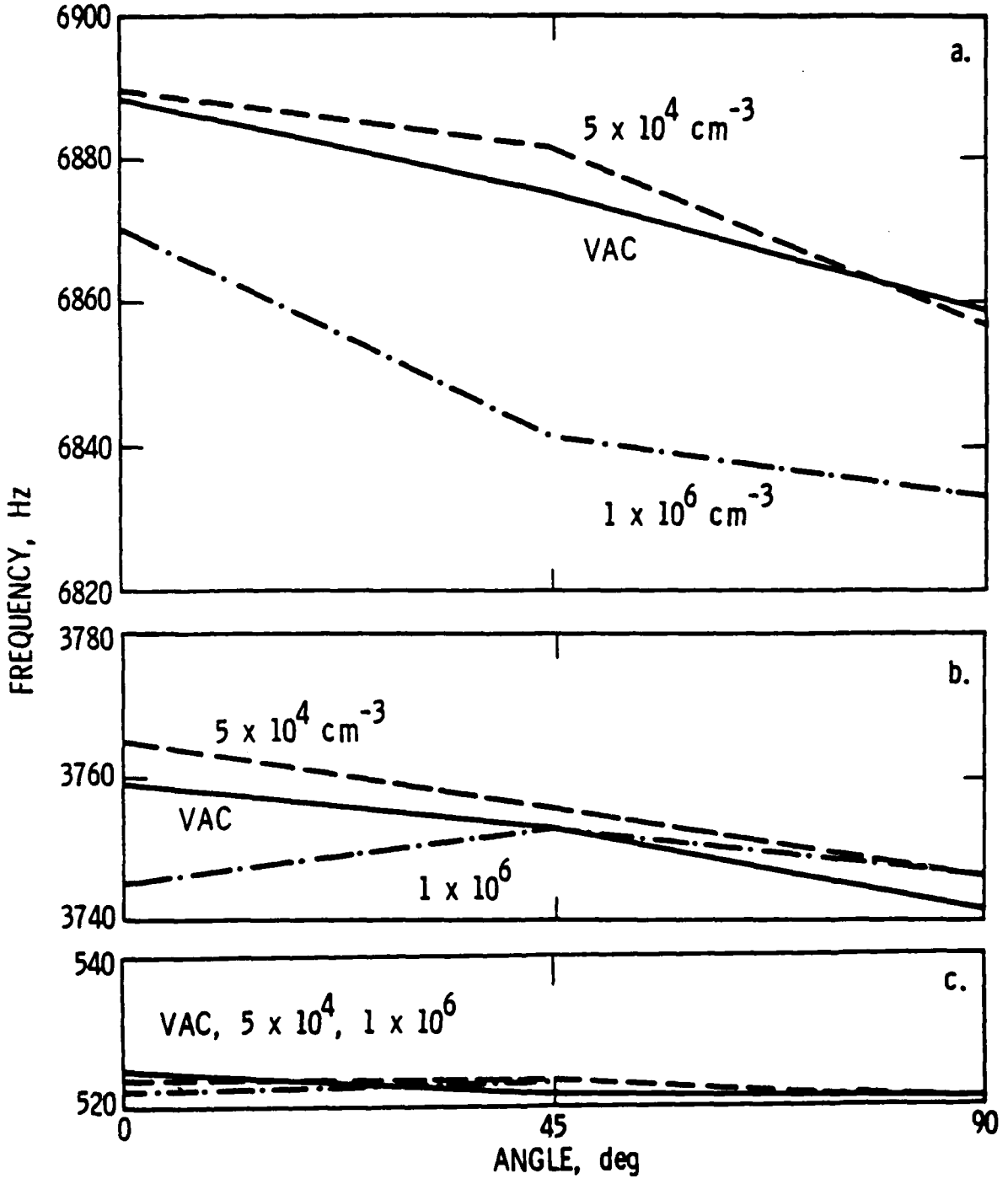

Fig. 12. Resonant frequency of the antenna circuit as a function of the angle between the antenna axis and the imposed external magnetic field for the antenna in vacuum and at plasma densities of 5×10^4 and 1×10^6 cm^{-3} for three different values of the tuning capacitance: (a) 79 μf, (b) 22 μf, and (c) 6.3 μf.

Table 3. Drive Current in Amps r.m.s. for the Data Shown in Fig. 3

	FREQUENCY, Hz				
	500	990	1845	3750	6860
Vacuum	27.0	23.5	21.4	14.0	10.4
8×10^4	25.2	25.1	23.4	23.4	10.1
1.2×10^6	25.5	25.0	24.1	11.1	5.7

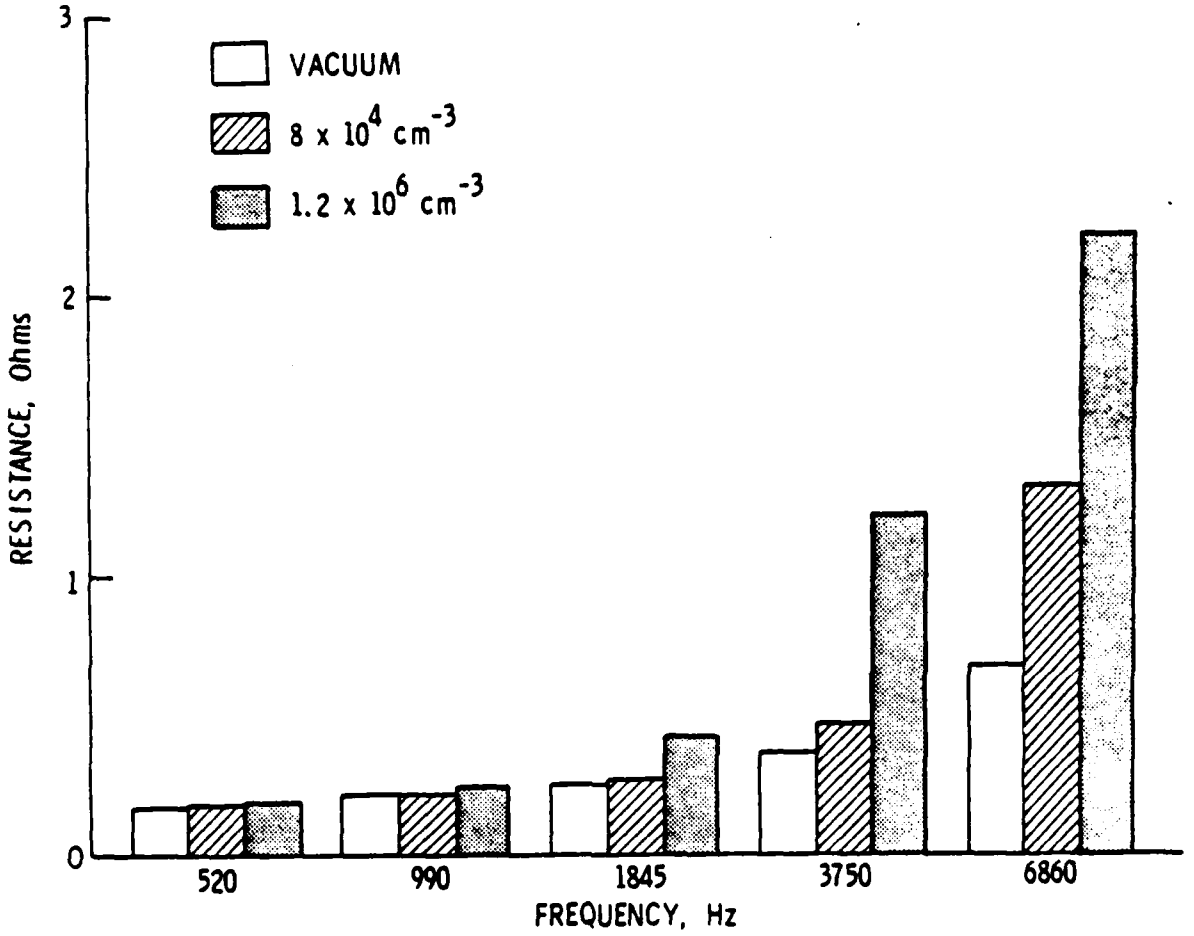

Fig. 13. Histogram of the antenna circuit series resistance at resonance for the five frequencies and three plasma conditions used in the plasma chamber tests.

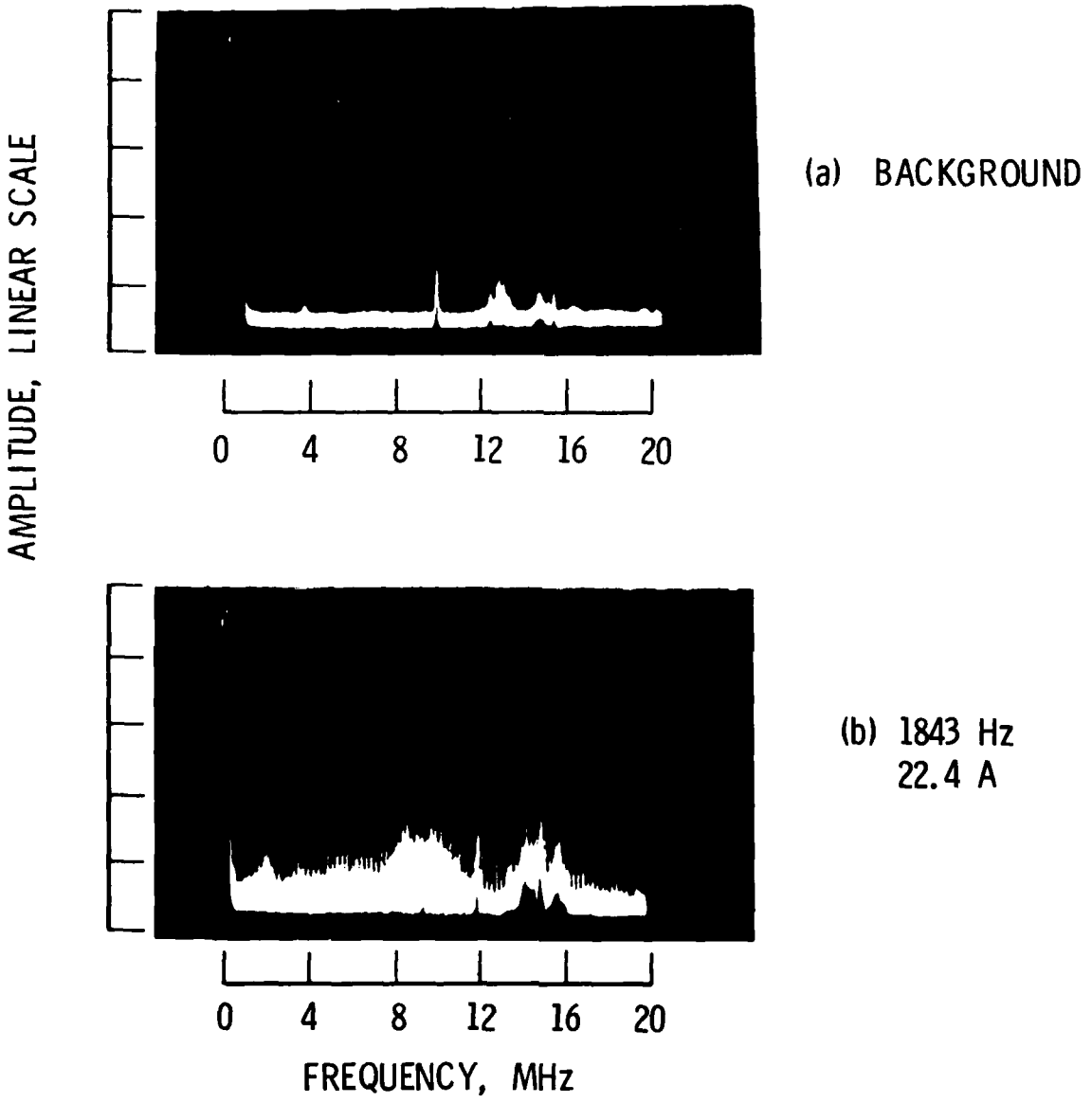

Fig. 14. Wave spectrum in plasma in the frequency range from 0 to 20 MHz. a) Background with no antenna current, b) Antenna current of 22.4 A RMS at 1843 Hz.

Fig. 13b shows the spectrum with the VLF antenna carrying 22.4 A at 1843 Hz. The broad feature near 9 MHz peaks near the plasma frequency. The "picket fence" structure in the spectrum is an artifact of the data presentation. The sweep rate of the spectrum analyzer was 5 ms/division. At 1843 Hz that is about 0.1 division per cycle. That is the spacing of the "picket fence" structure. We conclude that the wave turbulence in the MHz frequency range is being modulated almost 100% by the VLF signal on the antenna.

The increase in the circuit resistance is most likely due to power lost to plasma wave turbulence. The wave diagnostics were not designed to identify the wave modes. Scarf and Fredericks [1972] have described an energy dissipation process induced by large amplitude electric fields and by the transient production of unstable plasma distributions. These effects can not be quantitatively evaluated by theoretical analysis because the loop antenna geometry is too complex.

The a.c. magnetic field component of the near field was measured by small search coils at several locations about the antenna. The near magnetic field was directly proportional to antenna current and independent of the plasma density as expected from Ampere's law in Maxwell's equations.

VI. SUMMARY

A loop antenna configuration is being defined for a transmitter to radiate VLF waves within the ionosphere. A one-third scale model was tested in a space-plasma simulation chamber at NASA Lewis Research Center. The following results were obtained:

1. The resonant frequency of the antenna circuit was insensitive to the plasma density.

2. The series resistance of the circuit increases in the plasma. This increase is small below 1 kHz and large above 3 kHz. The increased resistance is attributed to power lost to plasma turbulence.

3. The intensity of the ac magnetic-field component in the near field of the antenna in the plasma is unchanged from its value in free space.

4. The impedance of the antenna is insensitive to the rotation angle with respect to the dc magnetic field. In particular no significant impedance variations occurred at angles of 0 and 90°.

These tests confirm that a full size antenna can be tuned using fixed capacitance. The losses to be expected from plasma turbulence with the full size system cannot be readily extrapolated from the scale model tests. In particular the voltage across the terminals of the full size antenna will be significantly larger than the voltages across the terminal of the model.

REFERENCES

Baker, D. J., H. Weil and L. S. Bearce, Impedance and Large Signal Excitation of Satellite-borne Antennas in the Ionosphere, IEEE Trans. Antennas Propagat., AP-21(5), 672-679, 1973.

Bell, T. F., and T. N. C. Wang, Radiation Resistance of a Small Filamentary Loop Antenna in a Cold Multicomponent Magnetoplasma, IEEE Trans. Antennas Propagat., AP-19(4), 517-522, 1971.

Grard, R. J. L., and J. K. E. Tunaley, The Impedance of the Electric Dipole Aerial on the FR-1 Satellite, Ann. Geophys., 24(1), 49-61, 1968.

Gurnett, D. A., G. W. Pfeiffer, R. A. Anderson, S. R. Mosier and D. P. Cauffman, Initial Observations of VLF Electric and Magnetic Fields with the Injun 5 Satellite, J. Geophys. Res., 74(19), 4631-4648, 1969.

Koons, H. C., and D. A. McPherson, Measurement of the Nonlinear Impedance of a Satellite-borne Electric Dipole Antenna, Radio Sci. 9(5), 547-557, 1974.

Koons, H. C., D. A. McPherson and W. B. Harbridge, Dependence of VLF Electric Field Antenna Impedance on Magnetospheric Plasma Density, J. Geophys. Res., 75(3), 2490-2502, 1970.

Leiphart, J. P., R. W. Zeek, L. S. Bearce and E. Toth, Penetration of the Ionosphere by Very-low-frequency Radio Signals - Interim Results of the LOFTI I Experiment, Proc. IRE, 50(1), 6-17, 1962.

Scarf, F. L., and R. W. Fredricks, "Transmission Losses Associated with Plasma Perturbations," in Proceedings of the Conference on Antennas and Trans-ionospheric Propagation as related to ELF/VLF Downlink Satellite Communications, NRL Rpt. 7462, Naval Research Laboratory, Washington, D. C., p. 123-135, 1972.

Shawhan, S. D., and D. A. Gurnett, VLF Electric and Magnetic Fields Observed with the Javelin 8.45 Sounding Rocket, J. Geophys. Res., 73(25), 5649-5664, 1968.

Shkarofsky, I. P., Nonlinear Sheath Admittance, Currents and Charges Associated with High Peak Voltage Drive on a VLF/ELF Dipole Antenna Moving in the Ionosphere, Radio Sci., 7, 503-523, 1972.

Wang, T. N. C., and T. F. Bell, On VLF Radiation Resistance of an Electric Dipole in a Cold Magnetoplasma, Radio Sci., 5(3), 605-610, 1970.

Wang, T. N. C., and T. F. Bell, VLF/ELF Input Impedance of an Arbitrarily Oriented Loop Antenna in a Cold Collisionless Multicomponent Magnetoplasma, IEEE Trans. Antennas Propagat.(Commun.), AP-20, 394-398, 1972.

☆ U.S. Government Printing Office: 1986 678-004/30412

LABORATORY OPERATIONS

The Aerospace Corporation functions as an "architect-engineer" for national security projects, specializing in advanced military space systems. Providing research support, the corporation's Laboratory Operations conducts experimental and theoretical investigations that focus on the application of scientific and technical advances to such systems. Vital to the success of these investigations is the technical staff's wide-ranging expertise and its ability to stay current with new developments. This expertise is enhanced by a research program aimed at dealing with the many problems associated with rapidly evolving space systems. Contributing their capabilities to the research effort are these individual laboratories:

Aerophysics Laboratory: Launch vehicle and reentry fluid mechanics, heat transfer and flight dynamics; chemical and electric propulsion, propellant chemistry, chemical dynamics, environmental chemistry, trace detection; spacecraft structural mechanics, contamination, thermal and structural control; high temperature thermomechanics, gas kinetics and radiation; cw and pulsed chemical and excimer laser development including chemical kinetics, spectroscopy, optical resonators, beam control, atmospheric propagation, laser effects and countermeasures.

Chemistry and Physics Laboratory: Atmospheric chemical reactions, atmospheric optics, light scattering, state-specific chemical reactions and radiative signatures of missile plumes, sensor out-of-field-of-view rejection, applied laser spectroscopy, laser chemistry, laser optoelectronics, solar cell physics, battery electrochemistry, space vacuum and radiation effects on materials, lubrication and surface phenomena, thermionic emission, photosensitive materials and infrared detectors, atomic frequency standards, and environmental chemistry.

Computer Science Laboratory: Program verification, program translation, performance-sensitive system design, distributed architectures for spaceborne computers, fault-tolerant computer systems, artificial intelligence, microelectronics applications, communication protocols, and computer security.

Electronics Research Laboratory: Microelectronics, solid-state device physics, compound semiconductors, radiation hardening; electro-optics, quantum electronics, solid-state lasers, optical propagation and communications; microwave semiconductor devices, microwave/millimeter wave measurements, diagnostics and radiometry, microwave/millimeter wave thermonic devices; atomic time and frequency standards; antennas, RF systems, electromagnetic propagation phenomena, space communication systems.

Materials Sciences Laboratory: Development of new materials: metals, alloys, ceramics, polymers and their composites, and new forms of carbon; nondestructive evaluation, component failure analysis and reliability; fracture mechanics and stress corrosion; analysis and evaluation of materials at cryogenic and elevated temperatures as well as in space and enemy-induced environments.

Space Sciences Laboratory: Magnetospheric, auroral and cosmic ray physics, wave-particle interactions, magnetospheric plasma waves; atmospheric and ionospheric physics, density and composition of the upper atmosphere, remote sensing using atmospheric radiation; solar physics, infrared astronomy, infrared signature analysis; effects of solar activity, magnetic storms and nuclear explosions on the earth's atmosphere, ionosphere and magnetosphere; effects of electromagnetic and particulate radiations on space systems; space instrumentation.

...

END

FILMED

3-86

DTIC